BBA - Biomembranes 1861 (2019) 183026

Contents lists available at ScienceDirect

BBA - Biomembranes

journal homepage: www.elsevier.com/locate/bbamem

Melting transitions in biomembranes

Tea Mužić[a], Fatma Tounsi[a], Søren B. Madsen[a], Denis Pollakowski[a], Manfred Konrad[b], Thomas Heimburg[a,*]

[a] Membrane Biophysics Group, Niels Bohr Institute, University of Copenhagen, Denmark
[b] Max-Planck-Institute for Biophysical Chemistry, Am Fassberg 11, Göttingen 37077, Germany

ARTICLE INFO

Keywords:
Thermodynamics
Elastic constants
Ions
E. coli
B. subtilis
Lung surfactant
Nerves

ABSTRACT

We investigated melting transitions in native biological membranes containing their membrane proteins. The membranes originated from *E. coli*, *B. subtilis*, lung surfactant and nerve tissue from the spinal cord of several mammals. For some preparations, we studied the pressure, pH and ionic strength dependence of the transition. For porcine spine, we compared the transition of the native membrane to that of the extracted lipids. All preparations displayed melting transitions of 10–20° below physiological or growth temperature, independent of the organism of origin and the respective cell type. We found that the position of the transitions in *E. coli* membranes depends on the growth temperature.

We discuss these findings in the context of the thermodynamic theory of membrane fluctuations close to transition that predicts largely altered elastic constants, an increase in fluctuation lifetime and in membrane permeability. We also discuss how to distinguish lipid melting from protein unfolding transitions. Since the feature of a transition slightly below physiological temperature is conserved even when growth conditions change, we conclude that the transitions are likely to be of major biological importance for the survival and the function of the cell.

1. Introduction

Lipid bilayers display melting transitions at a temperature T_m, during which both lateral and chain order. The transitions are accompanied by the absorption of excess heat, called the melting enthalpy. The typical transition temperatures range from − 20° to + 60 °C depending on chain length, chain saturation and the chemical nature of the head groups [1]. Melting transitions can easily be observed with calorimeters and various spectroscopic methods such as infrared spectroscopy or magnetic resonance. Mixtures of lipids with different melting temperatures display phase behavior, which can be displayed in phase diagrams [2]. These diagrams show the coexistence of phases as a function of both molar fractions of the components and intensive variables such as temperature and pressure. From the theoretical analysis of phase diagrams one can obtain melting profiles of the lipid mixtures, and understand the phase separation processes [1, 3]. Consequently, one finds domain formation in certain regimes of the phase diagram [4, 5].

It is little known that biological membranes also display melting transitions close to the physiological temperature regime. Several publications in the 1970s reported, for example, melting phenomena in the membranes of *Mycoplasma laidlawii* [6, 7], *Micrococcus lysodeikticus* [8], mouse fibroblast LM cells [9], and red blood cells [10]. Haest et al. [11] showed by electron microscopy that the arrangement of proteins in a native bacterial membrane correlates with this transition. Transitions have also been reported for lung surfactant [12-16] and *Escherichia coli* (*E. coli*) membranes [17]. However, the importance of these transitions for the function of cells has been little appreciated. Since biological membranes consist of hundreds or even thousands of components [18, 19], it seems impossible to construct phase diagrams. Due to Gibbs' phase rule, the possible number of coexisting phases is of similar order as the number of components when neglecting the phase boundaries. However, the compositions of domains cannot easily be derived from simple thermodynamics considerations or measurements if the finite size domains is taken into account, because the length of the domain interface adds further degrees of freedom. We show below that it is nevertheless possible to extract useful information from the melting profiles.

Melting transitions strongly influence elastic constants [20, 21]. According to the fluctuation-dissipation theorem, the heat capacity is proportional to enthalpy fluctuations. All other susceptibilities are similarly related to fluctuations of extensive variables. For instance, the

* Corresponding author.
E-mail address: theimbu@nbi.ku.dk (T. Heimburg).

https://doi.org/10.1016/j.bbamem.2019.07.014
Received 27 March 2019; Received in revised form 15 July 2019; Accepted 17 July 2019
Available online 26 August 2019

isothermal area compressibility is proportional to area fluctuations [20, 22] and the capacitance is proportional to charge fluctuations [23]. Further, in lipid systems the isothermal compressibility is proportional to the heat capacity [20, 21, 24]. The same is true for the other susceptibilities. They are all related to the heat capacity. Consequently, both heat capacity, compressibility and capacitive susceptibility are at a maximum in the melting transition [20, 23]. Heat capacity and area compressibility are also related to the bending elasticity [20, 25, 26], i.e., they are also at a maximum in a transition. The bending elasticity, however, is an important property for the fusion and fission of membranes [27]. This implies that endocytotic and exocytotic events are potentially enhanced in transitions.

Furthermore, the area compressibility is related to the permeability of membranes [28-31]. To create pores, the membrane in their surroundings has to be locally compressed, which is facilitated close to transitions [31, 32]. The pores in the membrane are also related to the formation of lipid ion channels, i.e., pores in the lipid membranes that display conduction patterns that are practically indistinguishable from protein channels [30, 31, 33-37]. The fluctuation-dissipation theorem demands that larger fluctuation amplitudes are accompanied by longer fluctuation lifetimes. This results in longer mean open-lifetimes of lipid pores in the transition range [38, 39]. The lifetimes of lipid membrane fluctuations span the range from milliseconds to seconds, and they are therefore just in the range observed for protein channel open-lifetimes.

It seems likely that transitions also influence dynamical properties of membranes. For instance, the sound velocity in lipid dispersions is a function of the membrane compressibility. As a consequence, sound velocities in transitions are reduced [24, 40]. Based on this observation, it has been proposed that the presence of a phase transition gives rise to the possibility of the propagation of solitary pulses (solitons) in cylindrical membranes that resemble action potentials [22, 41-43].

Various authors have shown that transitions are influenced by drugs, e.g., by anesthetics, neurotransmitters or peptides [39] but also by integral [44, 45] and peripheral proteins [46, 47]. Anesthetics lower the transition temperature of lipids by a well-known mechanism called melting-point depression [3, 48-50]. The observed pressure-reversal of anesthesia is well explained by the influence of hydrostatic pressure on melting transitions [50-52]. Within the soliton theory for the nerve pulse, the effect of anesthetics is explained by the increased free energy threshold for the induction of a phase transition [53]. For the above reasons, drugs and proteins potentially alter the elastic constants and the relaxation timescales [39] of membranes.

The striking influence of the lipid transition on membrane properties which are of biological relevance warrants a careful reevaluation of this phenomenon. In this work we investigate the melting in various biological membranes, including the bacteria *E. coli* and *Bacillus subtilis* (*B. subtilis*), lung surfactant, and nerve preparations from rat, sheep and pig. We show that the transitions in these systems are all very similar and are found 10–20° below growth or body temperature. If the growth temperature of bacteria is changed, the transitions shift as well in the same direction. We investigate the role of pressure and discuss the lifetimes of membrane perturbations. In the Discussion section we address the putative role of such transitions in biology.

2. Materials and methods

2.1. Lipids

Lipids were purchased from Avanti Polar Lipids (Birmingham, AL) and used without further purification. Bovine lung surfactant (BLES Biochemicals Inc., London, Ontario) was a gift from Prof Fred Possmeyer (London, Western Ontario). BLES (bovine lipid extract surfactant) is an organic extract of bovine surfactant from which cholesterol has been removed, together with certain other components. It contains small amounts of membrane soluble proteins (SP-B and SP-C) and 77 wt % of zwitterionic lipids. More than half of it is dipalmitoyl phosphatidylcholine (DPPC, 41% of total weight). The exact composition of BLES is given in [54]. CUROSURF (Chiesi Limited, Manchester, UK) is another clinically used surfactant preparation obtained from organic extracts of minced porcine lung tissue. CUROSURF was a gift from Søren Thor Larsen from Haldor Topsoe A/S (Denmark). It contains around 70–76 wt % zwitterionic phospholipids, about two-thirds of which is DPPC. The hydrophobic proteins SP-B and SP-C represent about 1% of the total weight. Details of the composition are given in [55]. CUROSURF initially contains a high proportion of blood and cell lipids contaminating the surfactant, which are in part eliminated by chromatographic procedures that also eliminates other components. As a consequence of their extraction and processing procedures, the two surfactants are similar but not identical to the native lung surfactant.

2.2. Bacterial cells

The *E.coli* strain XL1 blue with tetracycline resistance (Stratagene, La Jolla, CA) and *B. subtilis* were grown in an LB-medium at 37 °C. Bacterial cells were disrupted in a French Press at 1200 bars (Gaulin, APV Homogenizer GmbH, Lübeck, Germany) and centrifuged at low speed in a desk centrifuge to remove solid impurities. The remaining supernatant was centrifuged at high speed in a Beckmann ultracentrifuge (50,000 rpm) in a Ti70 rotor, or in a fast desktop centrifuge, to separate the membranes from soluble proteins and nucleic acids. The pellet was resuspended in buffer (33 vol% glycerol plus 67 vol% 10 mM Tris, 1 mM EDTA, pH 7.2) and centrifuged again. The membrane fractions in the pellets were measured in a calorimeter. The concentration of membranes in the calorimetric scan of *E. coli* membranes was 26.3 mg/ml as determined from the dry weight of the samples. Lipid melting peaks and protein unfolding profiles can easily be distinguished in pressure calorimetry due to their characteristic pressure dependencies, the pressure dependence of lipid transitions being much higher than that of proteins [21].

2.3. Rat central brain

Rat brains were donations from the Rigshospitalet in Copenhagen (Prof. Niels V. Olsen). They were kept in a freezer until use. We used the central brain and parts of the spinal cord. The central brain tissue was ground with mortar and pestle. The resulting liquid sample was diluted in a buffer (150 mM KCl, 3 mM Hepes, 3 mM EDTA, pH 7.2–7.4). Subsequently, the sample was sonicated with a high-power ultrasonic cell disruptor (Branson Ultrasonic cell disruptor B15, Danbury, CT, USA) in pulse mode to prevent heating of the sample. Finally, water soluble parts were washed away from the sample by centrifugation. The pellet was assumed to mainly consist of membranes as was apparent in pressure calorimetry (see Experimental results section). It was used for the calorimetric experiments. More details can be found in [56].

2.4. Mammalian spines

Sheep spines were bought from a local butcher and were kept on ice. The spine was opened with a saw and the spinal cord was removed. Using scissors and tweezers the dura mater which surrounds the spinal cord was removed. The spinal cord was cut into small pieces and homogenized over a period of 20 min with a stator rotor (Tissue Master 125 W Lab Homogenizer, Omni International, Inc, Kennesaw, GA) at 33.000 rpm with a 7 mm probe head in 30-second intervals with breaks of 30 s to prevent heating. The homogenate was dissolved in a buffer (150 mM NaCl, 1 mM Hepes, 2 mM EDTA, pH 7.4) and spun down in a desk centrifuge at 3360 g for 15 min. The sample was centrifuged using an MSE Super Minor centrifuge (England) at 3355 RCF in 15 min intervals. After each round the supernatant was discarded, tubes were filled up to the previous level with buffer, vortexed and put in the centrifuge for another cycle until the supernatant was completely clear. The majority of the fibrous tissue that sediments at the bottom was

removed by pouring the viscous pellet into a new tube after each centrifugation round.

Porcine spines were bought from the local butcher, and a homogenate of spinal cord tissue was prepared as for sheep spines. The homogenate was filtrated through a stainless steel 100 mesh with 140 μm opening size (Ted Pella, Inc, Redding, CA) in order to remove fibrous tissue. The homogenate was dissolved in a 150 mM NaCl 11.8 mM phosphate buffer, pH 7.4 and treated as in the sheep spine preparation. Details on sheep and porcine spine preparations can be found in [57] and [58].

2.5. Calorimetry

Heat capacity profiles were obtained using a VP scanning-calorimeter (MicroCal, Northampton, MA) at scan rates of 20°/h (for spinal cord of rats, sheep, and chicken) or 30°/h for lung surfactant, *E. coli* and *B. subtilis* membranes. This is much faster than the scan rate we typically use for pure lipids (typically ⩽5°/h). This is justified if the expected melting profiles are very broad, and the c_p maximum values are small. A faster scan rate increases the power of the calorimetric response and thus the strength of the signal. The small magnitude of the heat capacity leads to fast relaxation behavior [38, 39] which enables us to scan fast without hysteresis problems. Pressure calorimetry was performed in a steel capillary inserted into the calorimetric cell as previously described [21, 38]. In these experiments, absolute heat capacities are not given. In the porcine spine preparations, 30 vol% glycerol was added to the sample solution in order to prevent freezing of the sample at temperatures below 0 °C in the calorimeter. A crucial procedure in the analysis of heat capacity profiles with broad and weak signal is the subtraction of a baseline. It is shown in the supplementary information.

With all samples we performed both heating and cooling scans. Typically, the first scan was a heating scan from low temperature to about 38 °C, followed by a cooling scan. These scans were performed to equilibrate the sample without denaturing the proteins. They were not used for analysis. Subsequent scans were performed over the whole temperature range. In all figures in this work, heating scans are shown. For several of the preparations we display the heat capacity in arbitrary units. What we would like to know is the heat capacity per gram of overall lipid. The best manner to do so is to extract the lipid from a large preparation of membranes, and determine its weight. We did not succeed in obtaining reproducible numbers, probably because our samples were too small and the accuracy of our extraction was not high enough. Future studies will be directed towards obtaining absolute numbers for the heat capacity.

3. Theoretical considerations

In the following sections we outline why a maximum of the heat capacity is important for its physical properties, in particular for the membrane compressibility, its elasticity and the lifetime of membrane perturbations, and the lifetime of membrane pores.

3.1. Fluctuations, susceptibilities and fluctuation lifetimes

According to the fluctuation-dissipation theorem, the heat capacity of a membrane is related to enthalpy fluctuations [20] through

$$c_p = \left(\frac{\partial H}{\partial T}\right)_p = \frac{\langle H^2\rangle - \langle H\rangle^2}{kT^2}, \tag{1}$$

i.e., the mean square deviation of the enthalpy from its average value. Similarly, the isothermal volume compressibility is related to volume fluctuations [20],

$$\kappa_T^V = -\frac{1}{\langle V\rangle}\left(\frac{\partial V}{\partial p}\right)_T = \frac{\langle V^2\rangle - \langle V\rangle^2}{\langle V\rangle \cdot kT}, \tag{2}$$

and the isothermal area compressibility is related to area fluctuations,

$$\kappa_T^A = -\frac{1}{\langle A\rangle}\left(\frac{\partial A}{\partial \Pi}\right)_T = \frac{\langle A^2\rangle - \langle A\rangle^2}{\langle A\rangle \cdot kT}. \tag{3}$$

It is an empirical finding that for DPPC and some other lipids [21, 39]

$$V(T) \approx \gamma_V H(T) \quad ; \quad A(T) \approx \gamma_A H(T) \tag{4}$$

where $\gamma_V = 7.8 \cdot 10^{-10}\,\mathrm{m^2/N}$ [21] and $\gamma_A = 0.893\,\mathrm{m/N}$ [20] for DPPC. It has been shown that the parameters γ_V and γ_A are very similar for different lipids, lipid mixtures and even biological preparations such as lung surfactant. Using Eqs. (1)–(4), one can conclude that

$$\kappa_T^V = \frac{\gamma_V^2 \cdot T}{\langle V\rangle} c_p \quad ; \quad \kappa_T^A = \frac{\gamma_A^2 \cdot T}{\langle A\rangle} c_p \tag{5}$$

i.e., the excess compressibilities are proportional to the excess heat capacity changes. Molecular dynamics simulations suggest that these relations are also true for absolute heat capacities and the total compressibilities [59].

According to [20], [60], and [61], the bending elasticity κ_B (i.e., the inverse of the bending modulus) is proportional to the area compressibility,

$$\kappa_B = \frac{16}{\langle D\rangle^2}\kappa_T^A = \frac{16\gamma_A^2 T}{\langle D\rangle^2\langle A\rangle} c_p, \tag{6}$$

where D is the membrane thickness. Therefore, the bending elasticity is at a maximum in the melting transition. One can show that the bending elasticity is proportional to the curvature fluctuations.

Through the fluctuation-dissipation theorem, the fluctuations are also coupled to the relaxation time τ,

$$\tau = \frac{T^2}{L} c_p \tag{7}$$

where $L \approx 7 \cdot 10^8\,\mathrm{J\cdot K/mol\cdot s}$ for DPPC and DMPC vesicles [38, 39]. This implies that regions of high heat capacity display slow relaxation processes. Relaxation times are identical to fluctuation lifetimes [62]. Therefore, it has been suggested that these lifetimes correspond to the open-lifetimes of lipid ion channels, which are pores in the membrane with conductance signatures that are indistinguishable from those of protein ion channels [31, 37]. It has in fact been demonstrated experimentally that the channel lifetimes are related to the heat capacity not only for lipid membranes, but also for protein channels reconstituted into synthetic membranes displaying a transition close to experimental temperature [37, 63].

3.2. Pressure dependence of transitions and volume compressibility

The pressure dependence of lipid melting and protein unfolding is very different. Membranes generally increase their transition temperatures upon increase of hydrostatic pressure because the excess volume of the membrane is of the order of +4% and the melting temperature is roughly given by $T_m = (\Delta E + p\Delta V)/\Delta S$, i.e., it is proportional to the hydrostatic pressure. Protein unfolding transitions, in contrast, usually display a very small excess volume which is negative [64, 65]. A negative excess volume implies that pressure lowers the unfolding temperature of proteins. Therefore, they can be denatured by high pressure. This implies that lipid and protein transitions can be distinguished in calorimetric scans performed at different pressures.

For lipid membrane transitions it has been shown that if Eq. (4) is valid for all temperatures, one can deduce the relation between heat capacity and compressibility from heat capacity profiles obtained in the presence of a hydrostatic pressure difference, Δp. The enthalpy $\langle \Delta H\rangle_T^{\Delta p}$ obtained at excess pressure Δp can be superimposed with an enthalpy

profile obtained at $\Delta p = 0$ when the temperature T is rescaled to a new temperature T^* according to the following relations [21]:

$$\langle \Delta H \rangle_T^{\Delta p} = (1 + \gamma_V \cdot \Delta p) \langle \Delta H \rangle_{T^*}^{\Delta p=0} \quad \text{with} \quad T^* = \frac{T}{1 + \gamma_V \cdot \Delta p} \equiv f \cdot T, \tag{8}$$

This relation allows us to check two properties of lipid melting: 1. a proportional relation between excess volume and enthalpy that is valid for all temperatures and 2. the value of γ_V. If Eq. (8) leads to two superimposable c_p profiles, one can conclude that relations in Eq. (5) are also valid for biological preparations. We will use this relation below to determine γ_V for biological preparations, and to confirm that the proportional relation between excess compressibility and heat capacity is also valid for biological melting transitions.

A similar relation for the dependence of membranes on lateral pressure is very likely but more difficult to determine. There exists indirect evidence that the proportional relation between enthalpy and area, and the second relation in Eq. (5) are also correct [20, 25, 26, 59].

On small scales, biological membranes are heterogeneous and form domains which are usually very small. Our above statements are true for the total membrane system, i.e., on the scale of the membrane fragments from which the heat capacity was obtained. However, our theory does not make any assumptions about the local state of a membrane.

3.3. Reversibility of protein unfolding and lipid melting

Most proteins unfold irreversibly upon heating, which is a consequence of the aggregation of unfolded chains that expose hydrophobic residues to water. Since aggregation is a slow process, protein unfolding may be partially reversible on a short time scale or in consecutive scans. In contrast, lipid melting is always fully reversible. This allows us to distinguish protein unfolding from lipid melting in several consecutive heating scans in the calorimeter.

4. Experimental results

Here, we present studies on various types of cell membranes. These include two different lung surfactant preparations, *E. coli* and *B. subtilis* membranes, and three different brain and spine preparations from rat, sheep and pig.

4.1. Lung surfactant

Lung surfactant is a lipid film that exists in a monolayer-bilayer equilibrium on the surface of the alveoli of the lung [66, 67]. It reduces the surface tension of the air-water interface in the alveoli and prevents the lung from collapsing due to the capillary effect. It contains about 5% of surfactant-associated proteins (SP-A, B, C and D). The rest is lipids, predominantly DPPC (≈40%) with a melting temperature of 41.2 °C. In clinical applications, one often uses lipid extracts from the surfactant. Two commercial surfactants are bovine lipid extract surfactant (BLES) prepared from bovine lungs and CUROSURF extracted from porcine lungs containing about 2% hydrophobic proteins [54]. It consists mostly of phospholipids with minor contents of the hydrophobic proteins SP-B and SP-C. Since these preparations are close to native membrane preparations, nearly free of proteins, and available in larger quantities, they are a good starting material for the study of transitions. Due to the high content in DPPC, they can readily be compared to a pure DPPC dispersion.

Fig. 1 shows the heat capacity profiles of DPPC large unilamellar vesicles (LUV) (Fig. 1, left), CUROSURF lung surfactant extract in units of J/g·K (Fig. 1, center) and BLES (Fig. 1, right, top panel) in arbitrary units at three different pressures (1 bar, 100 bars and 196 bars). The integral of the c_p-profile of CUROSURF yields $\Delta H \approx 32$ J/g of surfactant. The true value is somewhat higher because the c_p-profile extends to a temperature below zero which is not accessible in our experiment. For comparison, the major lipid component of lung surfactant (DPPC) possesses a melting enthalpy for the main transition of $\Delta H = 45$ J/g, which is of similar order as the surfactant melting enthalpy. Therefore, we will in the following assume that the transition enthalpies of DPPC and of lung surfactant per gram are similar. The transition maximum of the surfactant is at 27 °C.

The right hand panel of Fig. 1 shows the pressure dependence of the transition profile of BLES with a transition maximum at 26.9 °C. The transition maximum and the half width of the profile at 1 bar are nearly identical to that of CUROSURF. The transition peaks shift towards higher temperatures upon increasing pressure while maintaining the shape of the profile. One can multiply the absolute temperature axis with a factor f (Eq. (8)) in order to superimpose the profiles recorded at the three different pressures (Fig. 1 right, bottom). The respective factors are $f = 0.9925$ for the 100 bar recording, and $f = 0.985$ for the 196 bar recording. Using Eq. (8), one can now determine a value for γ_V,

$$\gamma_V = \frac{1 - f}{f \cdot \Delta p}. \tag{9}$$

This calculation yields $\gamma_V = 7.6 \cdot 10^{-10}\,\mathrm{m^2/N}$ for the 100 bar measurement and $\gamma_V = 7.8 \cdot 10^{-10}\,\mathrm{m^2/N}$ for the 196 bar measurement. This is within error identical to the value determined for DPPC ($\gamma_V = 7.8 \cdot 10^{-10}\,\mathrm{m^2/N}$) obtained by Ebel et al. [21] (see this reference also for an estimation of the errors). This will allow us to make estimates for volume and area compressibilities of lung surfactant (see below), and the relaxation times following Eqs. (5) and (7).

For CUROSURF, we obtained a melting enthalpy comparable to that of DPPC LUV, and the factor γ_V was found to be nearly identical for DPPC LUV and BLES. Taking into account that additionally the transition maximum and the half width of the two lung surfactant preparations are nearly identical, we can make the following assumptions: The melting enthalpy and the factor $\gamma_V = 7.8 \cdot 10^{-10}\,\mathrm{m^2/J}$ are the same for the two lung surfactant preparations and DPPC. We assume that this is also true for the relation between area changes and enthalpy changes. We therefore estimate that $\gamma_A = 0.893$ m/N for the three preparations, and that the phenomenological constant in Eq. (7) is given by $L = 7 \cdot 10^8$ J·K/mol·s. We further assume that for specific volume and area, the values for DPPC listed in [20] are reasonably close to the values of the biological preparation. We can now calculate the excess volume compressibility, κ_T^V, the area compressibility, κ_T^A, and the (excess) relaxation times τ in the transition of CUROSURF (where the absolute heat capacity values are known); they are given in Fig. 2 and are compared to the DPPC LUV preparation. As shown above, the compressibilities and the relaxation times are roughly proportional to the excess heat capacity. For the maximum volume compressibility of DPPC LUV we find $\Delta\kappa_T^V = 33{\cdot}10^{-10}\,\mathrm{m^2/N}$, for the area compressibility $\Delta\kappa_T = 22$ m/N and for the relaxation time 0.94 s, respectively. For CUROSURF, we find $\Delta\kappa_T^V = 3.6{\cdot}10^{-10}\,\mathrm{m^2/N}$, for the area compressibility $\Delta\kappa_T = 2.4$ m/N and for the relaxation time 0.093 s. This implies that there is roughly a factor of 10 between DPPC LUV and lung surfactant, which is also reflected in the finding that the half width of the c_p profile is about 10-fold larger for CUROSURF than it is for DPPC LUV.

At physiological temperature, the lipid system (CUROSURF) is above its melting temperature and the excess heat capacity is close to zero. This implies that the relaxation times of the lung surfactant preparation at physiological temperature are in the millisecond regime. In the Discussion section we will argue that this time scale is related to the time scale of lipid ion channels and the time scale of the nerve impulse.

4.2. E. coli and B. subtilis membranes

In a second step, we prepared *E. coli* and *B. subtilis* membranes as described in the Materials and methods section. These *E. coli* cells have a tetracycline resistance, and the cultivation medium contains tetracycline to prevent growth of other species. The pelleted membranes were dissolved in a buffer (see Materials and methods section), filled

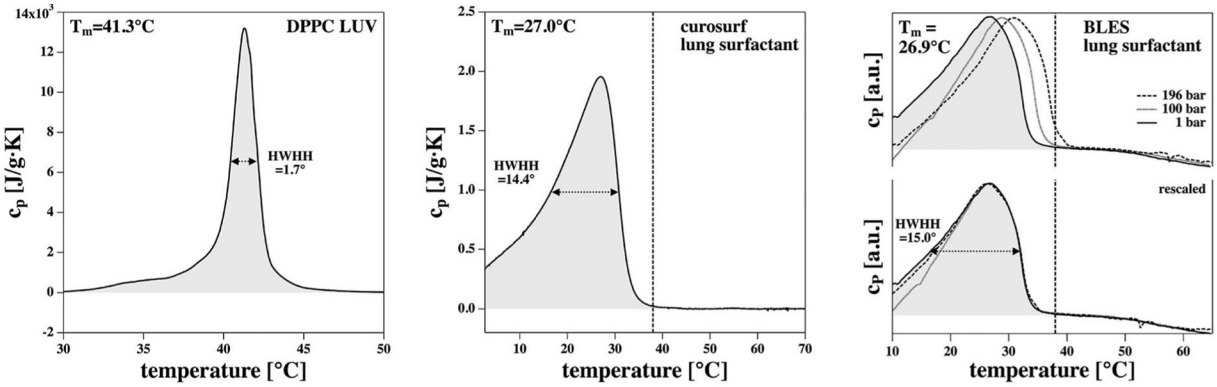

Fig. 1. Heat capacity profiles of lung surfactant. Left: DPPC large unilamellar vesicles (LUV). The half width of the peak is 1.7°. Center: CUROSURF, a lipid extract from porcine lungs. Half width is 14.4°. Right: Bovine lipid extract surfactant (BLES) as a function of pressure (top panel) and rescaled using Eq. (8) (bottom panel). The half width is 15.0°. Both lung surfactant preparations show a transition peak with a transition temperature of 26.9 °C.

into a calorimeter and scanned with 30°/h. In a first experiment, *E. coli* cells were grown at 37 °C. Fig. 3 (left) shows the first and the second calorimetric heating scan of the membranes in the range from 0 to 90 °C. The peak attributed to lipid melting is highlighted with grey shades. One recognizes four peaks above the growth temperature (at 48.7°, 54.5°, ~66° and ~88 °C), and one peak below growth temperature (~23 °C). The peaks above 37 °C become smaller in consecutive scans. This suggests that they can be attributed to partially irreversible protein unfolding. The peak at 21.3 °C is unchanged in the second scan. Its reversible nature suggests that it can be attributed to the lipid melting transition. The transition half width is 14.1 °C, which is nearly the same as for BLES and CUROSURF.

Fig. 3 (right) shows membranes from *B. subtilis* prepared in the same manner as the *E. coli* membranes. The protein peaks (at 49.7°, 60.4° and 69.8 °C) disappear in the second heating scan due to irreversible unfolding. The lipid transition temperature is about 13.6 °C and the half widths is 17.1°. This peak is still present in the second complete heating scan and is reversible. Thus, transitions in *B. subtilis* membranes are similar to those of the previous biological preparations in respect to half width.

Fig. 3 (center) shows the lipid peak of *E. coli* membranes at two different pressures (1 bar and 180 bars). At higher pressure, the position of the low temperature peak is shifted by 3.45° towards higher temperature. Using Eq. (9), one can rescale the temperature axis of the profile measured at excess pressure such that it is superimposed on the profile recorded at 1 bar. One finds that $\gamma_V = 6.5 \cdot 10^{-10}\,\mathrm{m^2/N}$, a value that is relatively close to that obtained for DPPC membranes and lung surfactant ($\gamma_V = 7.8 \cdot 10^{-10}\,\mathrm{m^2/N}$) [21]. In addition to the reversibility, this strongly suggests that the low temperature peak corresponds to lipid melting. As noted above, the excess volume of most protein unfolding reactions is negative and inconsistent with the observed pressure dependence of the low temperature peak. Overall, we find that the melting behavior of *E. coli* membranes is very similar to that of lung surfactant both in respect to width, transition temperature and to the ratio between excess enthalpy and excess volume. While not showing this here explicitly, we assume that also the total melting enthalpy per gram of the *E. coli* lipids is similar to that of DPPC and lung surfactant, and that one can draw similar conclusions with respect to the temperature dependence of the elastic constants and the time scale of the fluctuations.

In a further experiment, *E. coli* cells were grown at three different temperatures (15°, 37° and 50°, respectively, see Fig. 4). One can see that the melting peak of the lipid membrane (shown with grey shades) moves in the same direction as the growth temperature. T_g. The protein unfolding peaks are found at the same positions for $T_g = 15$ °C and $T_g = 37$ °C. This indicates that the cells adapt to different growth temperatures by changing the lipid composition. The protein unfolding peaks for $T_g = 50$ °C are somewhat different from those at the other two temperatures. This indicates that we may have selected a temperature-resistant mutant. Evolution of *E. coli* upon exposure to high growth temperatures has in fact been reported previously [68, 69].

Fig. 5 shows the dependence of the lipid melting transition on pH and NaCl concentration. Conditions are indicated in the figure legend. Upon lowering the pH from 9 to 5, the transition temperature increases by 7.6° (Fig. 5, left), which indicates that the *E. coli* membrane contains a significant fraction of negatively charged lipids. Fig. 5 (right) shows

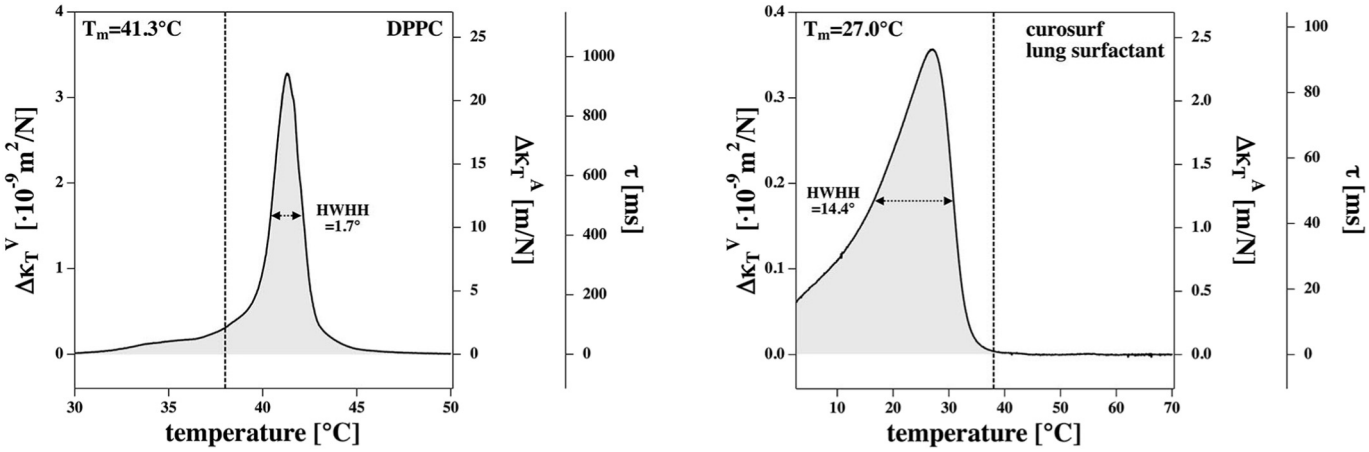

Fig. 2. Elastic constants and relaxation time scales calculated for DPPC large unilamellar vesicles (LUVs, left) and CUROSURF lung surfactant (right).

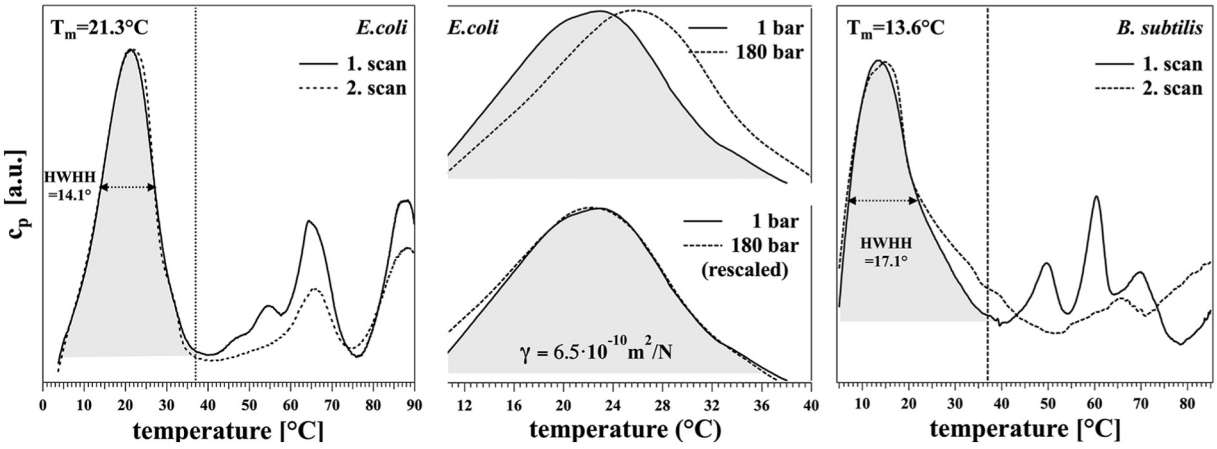

Fig. 3. Left: Heat capacity scans of *E. coli* membranes. In the second scan, the protein peaks are largely reduced. The lipid melting peak (grey shaded) is nearly identical on the first and the second scan. Center: The lipid melting peak at two different hydrostatic pressures (1 bar and 180 bars, top panel). The bottom panel shows that the c_p-profile rescaled according to Eq. (8) yields two nearly superimposable peaks with $\gamma_V = 6.5 \cdot 10^{-10}\,n^2/N$, which is very similar to the value for artificial lipids (DPPC: $7.8 \cdot 10^{-10}\,n^2/N$). Right: First and second calorimetric scan of *B. subtilis* membranes. Due to irreversible denaturation, the protein peaks disappear in the second scan.

the lipid melting peak at three different ionic strength conditions. Increase of the ionic strength from 25 mM NaCl to 300 mM NaCl leads to a slight decrease in transition temperature. This is expected from electrostatic theory [70] because Na^+ and Cl^- shield the electrostatic range of lipid charges.Therefore charged membranes are less protonated (see also Discussion section).

4.3. Nerve membranes

In the electromechanical theory for the action potential [22, 41, 43, 71], the melting transition plays a central role. Therefore, the investigation of melting profiles of nerve membranes is of particular importance. We have chosen central brain and spinal cord tissues because we assume that in these tissues most membranes are involved in signal conduction. However, we cannot distinguish different membranes. Our results represent an average over all types of membranes in the tissue. In contrast to soluble proteins (which can not be pelleted even up to > 100.000 g), membranes are easier to pellet. Therefore, our procedure attempts to separate soluble parts from the membranes. The membrane fraction analyzed here contains all membranes from the cells including those of organelles. We assume that a major fraction of the membranes are myelin sheets and axonal membranes.

Fig. 6 shows the heat capacity profiles for three different membrane preparations from the spinal cord of pig, the central brain (medulla and parts of the spinal cord) of rat and the spinal cord of sheep. The left panel shows the heat capacity profile of porcine spine membranes. It displays a maximum at 23.1 °C. There are two further peaks associated with protein unfolding located above physiological temperature (Table 1) that disappear in the second and third complete heating scan due to irreversible denaturation. The lipid peak in the third scan seems to be somewhat affected by the denaturation of the proteins, displaying a maximum at about 29 °C. Proteins aggregating upon denaturation diminish lipid-protein interactions. This would be consistent with the finding that extracted lipids display a c_p maximum at roughly the same temperature (bottom trace of the left hand panel). In this heat capacity profile one also finds a very sharp low enthalpy peak at around 51.5 °C. Such a sharp peak is typical for vesicles composed of a pure lipid component. Its origin is not clear and we disregard it due to its low enthalpy content. The center panel of Fig. 6 shows the membrane preparation from rat central brain. Here, we find a lipid membrane melting peak at around 28.2 °C, and two major protein unfolding peaks at 59 °C (with a minor shoulder at 50.2 °C), and 79.9 °C (Table 1) that disappear in the second complete heating scan due to irreversible denaturation of proteins. The right hand panel of Fig. 6 shows the calorimetric profile of sheep spine membranes that displays a lipid melting maximum at 24.1 °C) and protein unfolding peaks at 49.4, 56.7 and 83.3 °C). The protein peaks also disappear in a consecutive heating scan (data not shown because we could not identify a reasonable

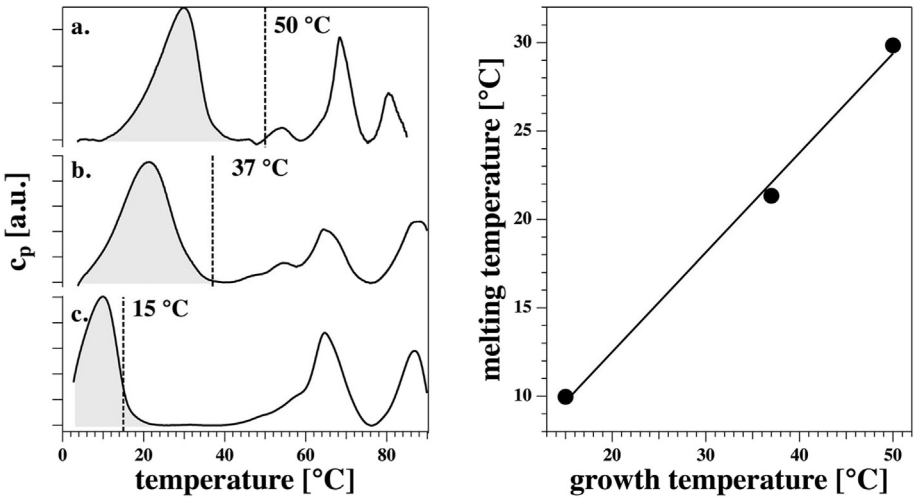

Fig. 4. Left: Adaptation of *E. coli* membranes to the growth temperature: 50 °C (a), 37 °C (b) and 15 °C (c). The lipid melting peak is shifted towards lower temperature upon decreasing the growth temperature. The protein unfolding peaks in (b) and (c) are identical while they are slightly different in (a). This indicates that the situations in (b) and (c) correspond to adaptation rather than to mutations. Right: Lipid melting peak maximum as a function of growth temperature.

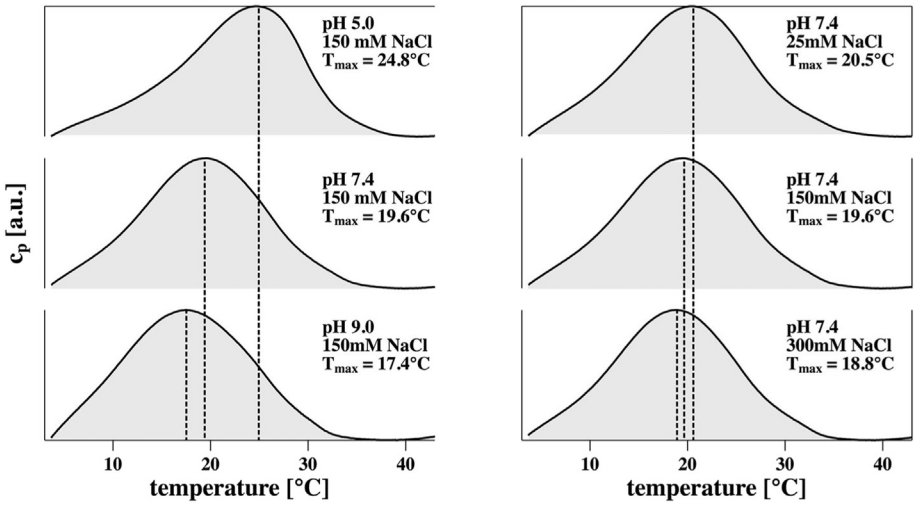

Fig. 5. Dependence of melting temperature of *E. coli* membranes on pH (left) and ionic strength (right).

baseline). We also investigated small amounts of chicken spine where similar calorimetric events as shown here for the other nerve preparations could be identified (data not shown). Summarizing one can state that the protein peaks are at similar positions in the three preparations, whereas the lipid peaks are not at exactly the same position. This may be an artifact due to heterogeneity of the biological sample preparations.

The half widths of the lipid peaks are of similar order as in the *E. coli*, *B. subtilis* and lung surfactant preparations. Even though we have not been able to measure absolute heat capacities due to the lack of knowledge of the amount of lipids in the sample, we assume that the overall magnitude of the heat capacity and the enthalpy changes are of comparable order as in lung surfactant (see Discussion section).

5. Discussion

We showed here that in all biological membrane preparations we have investigated one finds lipid melting transitions that occur about 10–20° below physiological or growth temperature. The preparations were from biological sources as different as Gram-negative and Gram-positive bacteria, lung surfactant and nerve membranes. In a recent publication, we have shown that such transitions also occur in cancer cells of various origins [72].

Table 1
Major peaks in the heat capacity profiles of native nerve preparations in the first complete heating scan.

	Pig	Rat	Sheep
Lipid	23.1	28.2	24.1
Protein	–	50.2	49.4
Protein	56.8	59.0	56.7
Protein	78.8	79.7	82.3

The lipid transitions can be identified by various indicators:

- In repeated scans over a large temperature interval the protein unfolding peaks are mostly irreversible while lipid melting transitions are reversible.
- Lipid transitions display a very different excess pressure dependence as compared to protein unfolding. While the excess volume of lipid transitions is positive, leading to an increase of the transition temperature of the order of 1°/40 bars (Figs. 1 and 3), the excess volume of proteins is usually negative indicating that the temperature of denaturation for proteins is lowered upon increasing pressure [64, 65].
- Comparison to melting profiles of lipid extracts (see Fig. 6) shows

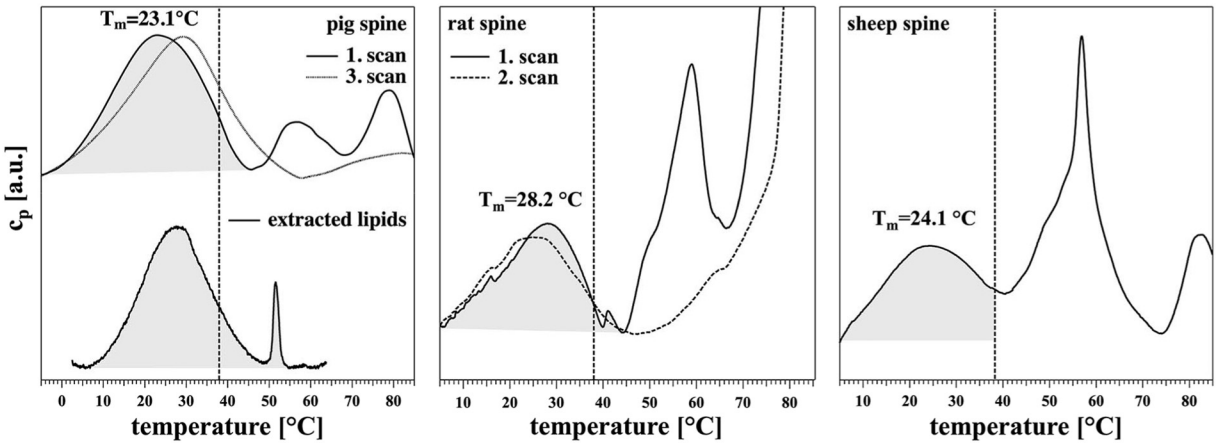

Fig. 6. Left, top: Heat capacity profiles of porcine spine membranes. The first scan shows the lipid melting peak and two major protein unfolding peaks. The latter peaks disappear in the third scan due to irreversible denaturation of the membrane proteins. Left, bottom: Heat capacity scan of the extracted membrane lipids of the same membrane preparation. Center: Melting profile of rat central brain membranes. The lipid membrane peak is conserved in the second scan while the protein unfolding is irreversible and the respective protein peaks disappear. From [56]. Right: Heat capacity profiles of sheep spine membranes. From [57] and [58].

that the melting peaks in the native preparations are similar with respect to transition temperature and transition half width.

The enthalpy of the protein unfolding transitions is of similar order as that of lipid melting, although exact ratios depend on the quality of the membrane preparations and the degree to which soluble proteins can be washed out of the samples.

We investigated various membrane preparations: two preparations of lung surfactant, membranes from the Gram-negative bacterium *E. coli*, characterized by an inner cytoplasmic membrane and an outer cell membrane, and the Gram-positive bacterium *B. subtilis*, displaying a cytoplasmic lipid membrane and an outer peptidoglycan layer, and three preparations from central brain and spinal cord nerves (pig, sheep and rat). In all of these preparations, we found lipid melting transitions in a range between 10 and 20° below standard growth or body temperatures. All of our preparations share some common features, such as displaying a transition width of about 10–15° and calorimetric events being detectable up to physiological temperature. Thus, the physiological temperature in all of the preparations was found to lie just between the lipid transition and the protein unfolding transitions such that minor perturbations of the membranes will move the membranes into the transition regime. It seems likely that the transition slightly below body temperature or growth temperature of bacterial cells, respectively, is a generic feature of most cell membranes, and this phenomenon may serve important purposes in the functioning of a cell. This feature is conserved from unicellular organisms like bacteria up to the complex nerve system of mammals.

For two of the biological preparations and the pure lipid DPPC, we measured the pressure dependence of the lipid transition. The pressure dependence yields a coefficient relating the excess volume and the excess enthalpy of the transitions, $V(T) = \gamma_V H(T)$ [21]. The constant γ_V was found to be $7.8 \cdot 10^{-10}\,m^2/N$ for DPPC [20, 21], $7.6–7.8 \cdot 10^{-10}\,m^2/N$ for the lung surfactant preparation (BLES) and $6.5 \cdot 10^{-10}\,m^2/N$ for *E. coli*. A value close to this was confirmed by Pedersen et al in MD-simulations even outside of the transition for DPPC [73]. This implies that the correlation between volume and enthalpy probably also holds outside of the transition regime. While these values are subject to some experimental deviations for the biological preparations as reflected by the broad transition peaks and uncertainties of baseline subtraction, they are reasonably similar for DPPC, lung surfactant and *E. coli* membranes. Further, we found that the overall excess enthalpy of the transition of lung surfactant was similar to that of DPPC. These two facts have an important consequence: the excess volume compressibility can now be determined from the heat capacity profile when the overall excess enthalpy of the transition and the magnitude of the excess heat capacity are known: $\kappa_T^V = (\gamma_V^2 T/V)\cdot c_p$ [20]. This implies that the membrane volume is more compressible in the melting transition. We assume the same proportionality to be true for the membrane area (excluding the membrane part of proteins): $A(T) = \gamma_A \cdot H(T)$, with $\gamma_A = 0.893\,m^2/J$ for DPPC [20]. Thus, we can calculate the changes in area compressibility from the heat capacity to be $\kappa_T^A = (\gamma_A^2 T/A)\cdot c_p$ [20]. The latter correlation also allows determination of changes in the bending elasticity (the inverse bending modulus in Helfrich's theory) to be $\kappa_B = (16\gamma_A^2 T/D^2 A)\cdot c_p$ [20]. The heat capacity is also correlated to the sound velocity. The velocity of sound in the membrane plane is given by $c = \sqrt{1/\rho_A \cdot \kappa_S^A}$, where κ_S^A is the adiabatic area compressibility. It is related to the isothermal compressibility via $\kappa_S^A = \kappa_T^A - (T/Vc_p)\cdot(dV/dT_p)^2$. Here, both κ_T^A, the volume expansion coefficient are simple functions of the heat capacity. Therefore, the sound velocity can be determined from the heat capacity profile [20, 24, 74]. By analogy, we assume this to be correct in the membrane plane, where the sound velocity in the fluid membrane is given by 176 m/s [22]. It is significantly slower in the transition regime.

We also found that in *E. coli* membranes that the melting temperature increases with decreasing pH. This is a consequence of protonation of charged lipids that lead to a reduction of electrostatic repulsion within the membrane plane. We also found that an increased ionic strength decreases the melting temperature. Electrostatics is shielded by ions. Therefore, our finding seems counterintuitive because one expects a similar effect as for increasing the proton concentration. However, sodium ions also have an effect on protonation. According to the well-known work of Träuble et al. [70], the pK_A of protonation curves of charged membranes decreases with increasing ionic strength. This implies that at higher ionic strength, the binding of protons is inhibited due to electrostatic shielding and the membrane effectively contains more charged lipids. Träuble et al. support their surprising theoretical prediction by experimental data. In agreement with our findings, they find in model membranes that the melting temperature decreases with increasing ionic strength. Therefore, our data are consistent Träuble's electrostatic theory.

Our findings have important consequences as summarized below. Many of them have been confirmed for synthetic lipid membranes.

- at the transition temperature, the volume and the lateral compressibility are at maximum, i.e., the membranes are more compressible within the transition [20, 60]
- the bending elasticity is at maximum, i.e., membranes in the transition range are much more flexible than in the fluid or gel membrane [20, 26]
- membrane lifetimes such as open dwell-time of membrane pores or curvature fluctuation lifetimes are longer within the transition
- the sound velocity is at a minimum [24, 40]
- the magnitude of the effects is similar for all biological preparations shown here because they display similar shapes of their transitions, both with respect to transition temperature and half width of the transition.
- since thickness and area of membranes change, transitions can also affect the capacitance of the membrane [23, 75]. We have previously shown that the capacitance in an artificial membrane can double when going from the gel to the fluid phase [76]. We have predicted that for a membrane exposed to transmembrane voltage, the capacitance can display a maximum in the transition [23].

There is good reason to assume that the above effects also exist for biological membranes, but they will be less pronounced because the heat capacity at maximum is lower and the width of the transition is considerably larger. For membrane function this implies that

- the probability for membrane fusion and fission events is enhanced because it depends on curvature elasticity [27]
- membrane pores are more abundant because their energy depends on the lateral compressibility [31, 32]
- lateral sound pulses called solitons can be generated in membranes [22]
- anesthetics, hydrostatic pressure or pH shift the transition and thereby generate changes in compressibility, bending elasticity, pore formation probability [30, 31, 36], open lifetime of membrane pores [36] and soliton excitability [53]. For instance, it has been shown that anesthetics can reduce the open probability of lipid channels in artificial membranes in the complete absence of proteins [30, 33].

Our data on *E. coli* membranes show that the lipid melting peak adapts to the growth temperature. If the latter is higher, the lipid transition also moves upwards in temperature in order to maintain a certain distance from physiological temperature. Adaptation of the transition temperature in *E. coli* membranes was reported previously [17]. The lung surfactant of hibernating squirrels displays a lower melting temperature than that of squirrels in summer [15, 16]. It seems likely that the adaptation consists of a change in the fraction of lipids with high and low melting temperatures, or the ratio of saturated to unsaturated chains [77]. In particular, for trout livers the lipid

composition was shown to be different in winter and summer [78]. At 20 °C, the fraction of saturated lipids is higher, whereas at 5 °C the fraction of poly-unsaturated lipids is higher. This was also found for the hibernating squirrels in [15] and [16]. The composition of lipid membranes also adapts to the presence of solvents (among those: acetone, chloroform or benzene) [79] or to hydrostatic pressure in deep sea bacteria [80]. High pressure increases the melting transition temperature. Consequently, the fraction of unsaturated lipids increases because these lipids display lower melting temperatures which opposes the pressure-effect. For this reason it seems from the few experimental studies reported so far that the relative position of the melting transition relative to physiological temperature is a property actively maintained by the organisms.

During a melting transition, membranes display a coexistence of gel and fluid phases that are easy to observe in fluorescence microscopy. This has been well documented for artificial membranes [4, 5, 81, 82], monolayers [83-86] and also for lung surfactant [13, 14]. Phase coexistence is obvious from fluorescence microscopy at the transition temperature, and domains are large. Domain coexistence has frequently been discussed in connection with so-called lipid rafts [87]. Rafts are rich in sphingomyelin, cholesterol and certain proteins [88-91]. Sphingolipids are known to display high melting temperatures, which are further enhanced by cholesterol. It is therefore tempting to assume that lipid rafts are gel domains swimming in a fluid environment. The fact that physiological temperature is at the upper end of the lipid melting transitions suggests that domains at physiological conditions must be small. This may be the origin of the difficulties to identify rafts at physiological conditions. If rafts are indicators for lipid melting processes, it is likely that they will be larger and much easier to detect 10–20° below body temperatures.

We and others have shown in the past that the melting transition of synthetic membranes shifts towards lower temperatures upon application of general and local anesthetics [3, 48, 50, 92]. This phenomenon follows the simple freezing-point depression law that relates the concentration of anesthetic in the fluid phase to the shift in transition temperature. This simple law has two advantages: 1. It is consistent with the famous Meyer-Overton correlation [50, 93] and 2. It is drug-unspecific, meaning that it does not depend on the particular chemistry of the anesthetic molecules. In connection with the present investigation we found that the anesthetic pentobarbital lowers transition temperatures in ovine and porcine spine by 2 to 3° when exposed to a buffer with up to 20 mol% pentobarbital (data not shown). A shift of about 3° was found for 8 mM pentobarbital on DPPC membranes [3]. Thus, the effect reported here is of similar order of magnitude. Since our biological preparations are subject to preparational variations and due to the additional effect of sample aging, we take this as a strong indication that the effect of anesthetics in biological preparations is similar to that in artificial membranes. We will investigate this effect more carefully in future studies. Altogether, our results are consistent with the finding that alcohols from ethanol to decanol lower the critical temperature of plasma membranes from rat leukemia cells [94].

An important consequence of the heat capacity maximum is the accompanying increase in the elastic susceptibilities, leading to more flexible and compressible membranes but also to a decrease in the sound velocity along membrane cylinders. This temperature and density dependence of the lateral sound velocity is the key element of the soliton theory for nerves that reproduces many properties of action potentials [22, 41-43, 71]. In this model for signal propagation, the nerve pulse is a solitary pulse in which the lateral density and membrane thickness transiently increases. Both effects have been found in experiments [95-98]. Recently, a theory was put forward that explains how anesthetics can change the stimulation threshold for these density pulses [53].

An important caveat in the interpretations of our data is that they are not obtained from clean membrane preparations. Our lung surfactant preparations are extracts that are close but not identical to native surfactant (see Materials and methods section). Native surfactant displays melting profiles of similar width but melting points between 30° and 33 °C [13, 14]. This is some degrees higher than determined in our surfactant preparations, probably due to the higher content of cholesterol. The *E. coli* preparation does not distinguish between inner and outer membrane, and the nerve preparations do not distinguish between the membranes of the axon, the myelin sheet and the membranes of the organelles. However, we consider these preparations to be close to biological membranes and expect, that in any clean preparation, the effects reported here will be more pronounced.

6. Conclusions

We have shown in this work that the lipid melting transitions exist in various biological membranes in vitro. They influence various mechanical features, which as a consequence influence membrane properties such as vesicle fusion probability, pore formation probabilities and their lifetimes, and the generation of solitary pulses in axonal membranes. Since the position of a transition depends on the presence of drugs, pH, pressure, or the presence of proteins, nature gains a powerful tool to influence cell membrane function via the control of macroscopic thermodynamic properties of the biological membrane as a whole. Due to their cooperative nature, these properties are impossible to understand in terms of biochemical pathways.

Author contributions

TM and FT prepared sheep and pig membranes from spinal cord and investigated them calorimetrically, SM prepared and investigated rat membranes from central brain, DP performed some of the calorimetric *E. coli* and *B. subtilis* measurements, MK prepared all *E. coli* and *B. subtilis* membranes. TH performed *E. coli*, *B. subtilis* and lung surfactant experiments and wrote the article. The article was proofread and commented by all co-authors.

Transparency document

The Transparency document associated with this article can be found, in online version.

Acknowledgments

M. Konrad acknowledges continuous support by the Max-Planck-Institute for Biophysical Chemistry. We thank Niels Olsen from Rigshospitalet Copenhagen for donations of rat brains. We thank Søren Thor Larsen (Haldor Topsoe A/S, Technical University of Denmark and University of Copenhagen) for a donation of CUROSURF lung surfactant, and Fred Possmeyer for a donation of lung surfactant preparations (BLES). A few data sets were used in a different context before. Two of the scans in Fig. 4 were used in [1]. The scans in the right panel of Fig. 1 were used in [21]. We added them for completeness of the discussion. This work was supported by the Villum Foundation (VKR 022130).

Appendix A. Supplementary data

Supplementary data to this article can be found online at https://doi.org/10.1016/j.bbamem.2019.07.014.

References

[1] T. Heimburg, Thermal Biophysics of Membranes, Wiley VCH, Berlin, Germany, 2007.
[2] A.G. Lee, Lipid phase transitions and phase diagrams. II. Mixtures involving lipids, Biochim. Biophys. Acta 472 (1977) 285–344.
[3] K. Græsbøll, H. Sasse-Middelhoff, T. Heimburg, The thermodynamics of general and local anesthesia, Biophys. J. 106 (2014) 2143–2156.
[4] J. Korlach, J.P. Schwille, W.W. Webb, G.W. Feigenson, Characterization of lipid

bilayer phases by confocal microscopy and fluorescence correlation spectroscopy, Proc. Natl. Acad. Sci. U. S. A. 96 (1999) 8461–8466.
[5] L.A. Bagatolli, E. Gratton, Two-photon fluorescence microscopy observation of shape changes at the phase transition in phospholipid giant unilamellar vesicles, Biophys. J. 77 (1999) 2090–2101.
[6] J.M. Steim, M.E. Tourtellotte, J.C. Reinert, R.N. McElhaney, R.L. Rader, Calorimetric evidence for the liquid-crystalline state of lipids in a biomembrane, Proc. Natl. Acad. Sci. U. S. A. 1963 (1969) 104–109.
[7] J.C. Reinert, J.M. Steim, Calorimetric detection of a membrane-lipid phase transition in living cells, Science 168 (1970) 1580–1582.
[8] G.B. Ashe, J.M. Steim, Membrane transitions in gram-positive bacteria, Biochim. Biophys. Acta 233 (1971) 810–814.
[9] B.J. Wisnieski, J.G. Parkes, Y.O. Huang, C.F. Fox, Physical and physiological evidence for two phase transitions in cytoplasmic membranes of animal cells, Proc. Natl. Acad. Sci. U. S. A. 71 (1974) 4381–4385.
[10] E.I. Chow, S.Y. Chuang, P.K. Tseng, Detection of a phase-transition in red-cell membranes using positronium as a probe, Biochim. Biophys. Acta 646 (1981) 356–359.
[11] C.W. Haest, A.J. Verkleij, J. de Gier, R. Scheek, P. Ververgaert, L.L.M. van Deenen, The effect of lipid phase transitions on the architecture of bacterial membranes, Biochim. Biophys. Acta 356 (1974) 17–26.
[12] K. Nag, J. Perez-Gil, M.L.F. Ruano, L.A.D. Worthman, J. Stewart, C. Casals, K.K.M.W. Keough, Phase transitions in films of lung surfactant at the air-water interface, Biophys. J. 74 (1998) 2983–2995.
[13] J. Bernardino de la Serna, J. Perez-Gil, A.C. Simonsen, L.A. Bagatolli, Cholesterol rules: direct observation of the coexistence of two fluid phases in native pulmonary surfactant membranes at physiological temperatures, J. Biol. Chem. 279 (2004) 40715–40722.
[14] J. Bernardino de la Serna, G. Orädd, L. Bagatolli, A.C. Simonsen, D. Marsh, G. Lindblom, J. Perez-Gil, Segregated phases in pulmonary surfactant membranes do not show coexistence of lipid populations with differentiated dynamic properties, Biophys. J. 97 (2009) 1381–1389.
[15] L.N.M. Suri, L. McCaig, M.V. Picardi, O.L. Ospina, R.A.W. Veldhuizen, J.F. Staples, F. Possmeyer, L.-J. Yao, J. Perez-Gil, S. Orgeig, Adaptation to low body temperature influences pulmonary surfactant composition thereby increasing fluidity while maintaining appropriately ordered membrane structure and surface activity, Biochim. Biophys. Acta 1818 (2012) 1581–1589.
[16] L.N.M. Suri, A. Cruz, R.A.W. Veldhuizen, J.F. Staples, F. Possmayer, S. Orgeig, J.J. Perez-Gil, Adaptations to hibernation in lung surfactant composition of 13-lined ground squirrels influence surfactant lipid phase segregation properties, Biochim. Biophys. Acta 1828 (2013) 1707–1714.
[17] H. Nakayama, T. Mitsui, M. Nishihara, M. Kito, Relation between growth temperature of *E. coli* and phase transition temperatures of its cytoplasmic and outer membranes, Biochim. Biophys. Acta 601 (1980) 1–10.
[18] S.H. White, T.E. Thompson, Capacitance, area, and thickness variations in thin lipid films, Biochim. Biophys. Acta 323 (1973) 7–22.
[19] G.A. Jamieson, D.M. Robinson, Mammalian Cell Membranes, vol. 2, Butterworth, London, 1977.
[20] T. Heimburg, Mechanical aspects of membrane thermodynamics. Estimation of the mechanical properties of lipid membranes close to the chain melting transition from calorimetry, Biochim. Biophys. Acta 1415 (1998) 147–162.
[21] H. Ebel, P. Grabitz, T. Heimburg, Enthalpy and volume changes in lipid membranes. I. The proportionality of heat and volume changes in the lipid melting transition and its implication for the elastic constants, J. Phys. Chem. B 105 (2001) 7353–7360.
[22] T. Heimburg, A.D. Jackson, On soliton propagation in biomembranes and nerves, Proc. Natl. Acad. Sci. U. S. A. 102 (2005) 9790–9795.
[23] T. Heimburg, The capacitance and electromechanical coupling of lipid membranes close to transitions. The effect of electrostriction, Biophys. J. 103 (2012) 918–929.
[24] W. Schrader, H. Ebel, P. Grabitz, E. Hanke, T. Heimburg, M. Hoeckel, M. Kahle, F. Wente, U. Kaatze, Compressibility of lipid mixtures studied by calorimetry and ultrasonic velocity measurements, J. Phys. Chem. B 106 (2002) 6581–6586.
[25] E. Evans, R. Kwok, Mechanical calorimetry of large dimyristoylphosphatidylcholine vesicles in the phase transition region, Biochemistry 210 (1982).
[26] R. Dimova, B. Pouligny, C. Dietrich, Pretransitional effects in dimyristoylphosphatidylcholine vesicle membranes: optical dynamometry study, Biophys. J. 79 (2000) 340–356.
[27] Y. Kozlovsky, M.M. Kozlov, Stalk model of membrane fusion: solution of energy crisis, Biophys. J. 82 (2002) 882–895.
[28] D. Papahadjopoulos, K. Jacobson, S. Nir, T. Isac, Phase transitions in phospholipid vesicles. Fluorescence polarization and permeability measurements concerning the effect of temperature and cholesterol, Biochim. Biophys. Acta 311 (1973) 330–340.
[29] M.C. Sabra, K. Jørgensen, O.G. Mouritsen, Lindane suppresses the lipid-bilayer permeability in the main transition region, Biochim. Biophys. Acta 1282 (1996) 85–92.
[30] A. Blicher, K. Wodzinska, M. Fidorra, M. Winterhalter, T. Heimburg, The temperature dependence of lipid membrane permeability, its quantized nature, and the influence of anesthetics, Biophys. J. 96 (2009) 4581–4591.
[31] T. Heimburg, Lipid ion channels, Biophys. Chem. 150 (2010) 2–22.
[32] J.F. Nagle, H.L. Scott, Lateral compressibility of lipid mono- and bilayers. Theory of membrane permeability, Biochim. Biophys. Acta 513 (1978) 236–243.
[33] K. Wodzinska, A. Blicher, T. Heimburg, The thermodynamics of lipid ion channel formation in the absence and presence of anesthetics. BLM experiments and simulations, Soft Matter 5 (2009) 3319–3330.
[34] B. Wunderlich, C. Leirer, A. Idzko, U.F. Keyser, V. Myles, T. Heimburg, M. Schneider, Phase state dependent current fluctuations in pure lipid membranes, Biophys. J. 96 (2009) 4592–4597.
[35] K.R. Laub, K. Witschas, A. Blicher, S.B. Madsen, A. Lückhoff, T. Heimburg, Comparing ion conductance recordings of synthetic lipid bilayers with cell membranes containing TRP channels, Biochim. Biophys. Acta 1818 (2012) 1–12.
[36] A. Blicher, T. Heimburg, Voltage-gated lipid ion channels, PLoS One 8 (2013) e65707.
[37] L.D. Mosgaard, T. Heimburg, Lipid ion channels and the role of proteins, Acc. Chem. Res. 46 (2013) 2966–2976.
[38] P. Grabitz, V.P. Ivanova, T. Heimburg, Relaxation kinetics of lipid membranes and its relation to the heat capacity, Biophys. J. 82 (2002) 299–309.
[39] H.M. Seeger, M.L. Gudmundsson, T. Heimburg, How anesthetics, neurotransmitters, and antibiotics influence the relaxation processes in lipid membranes, J. Phys. Chem. B 111 (2007) 13858–13866.
[40] S. Halstenberg, T. Heimburg, T. Hianik, U. Kaatze, R. Krivanek, Cholesterol-induced variations in the volume and enthalpy fluctuations of lipid bilayers, Biophys. J. 75 (1998) 264–271.
[41] T. Heimburg, A.D. Jackson, On the action potential as a propagating density pulse and the role of anesthetics, Biophys. Rev. Lett. 2 (2007) 57–78.
[42] S.S.L. Andersen, A.D. Jackson, T. Heimburg, Towards a thermodynamic theory of nerve pulse propagation, Progr. Neurobiol. 88 (2009) 104–113.
[43] B. Lautrup, R. Appali, A.D. Jackson, T. Heimburg, The stability of solitons in biomembranes and nerves, Eur. Phys. J. E 34 (2011) 57.
[44] E. Freire, T. Markello, C. Rigell, P.W. Holloway, E. Freire, T. Markello, C. Rigell, P.W. Holloway, Calorimetric and fluorescence characterization of interactions between cytochrome b_5 and phosphatidylcholine bilayers, Biochemistry 28 (1983) 5634–5643.
[45] M.R. Morrow, J.H. Davis, F.J. Sharom, M.P. Lamb, Studies of the interaction of human erythroyte band 3 with membrane lipids using deuterium nuclear magnetic resonance and differential scanning calorimetry, Biochim. Biophys. Acta 858 (1986) 13–20.
[46] T. Heimburg, R.L. Biltonen, A Monte Carlo simulation study of protein-induced heat capacity changes, Biophys. J. 70 (1996) 84–96.
[47] T. Heimburg, D. Marsh, Thermodynamics of the interaction of proteins with lipid membranes, in: K.M. Merz (Ed.), Biological Membranes: A Molecular Perspective From Computation and Experiment, Birkhäuser, Boston, 1996, pp. 405–462.
[48] Y. Kaminoh, S. Nishimura, H. Kamaya, I. Ueda, Alcohol interaction with high entropy states of macromolecules: critical temperature hypothesis for anesthesia cutoff, Biochim. Biophys. Acta 1106 (1992) 335–343.
[49] D.P. Kharakoz, Phase-transition-driven synaptic exocytosis: a hypothesis and its physiological and evolutionary implications, Biosci. Rep. 210 (2001) 801–830.
[50] T. Heimburg, A.D. Jackson, The thermodynamics of general anesthesia, Biophys. J. 92 (2007) 3159–3165.
[51] J.R. Trudell, D.G. Payan, J.H. Chin, E.N. Cohen, The antagonistic effect of an inhalation anesthetic and high pressure on the phase diagram of mixed dipalmitoyldimyristoylphosphatidylcholine bilayers, Proc. Natl. Acad. Sci. U. S. A. 72 (1975) 210–213.
[52] H. Kamaya, I. Ueda, P.S. Moore, H. Eyring, Antagonism between high pressure and anesthetics in the thermal phase transition of dipalmitoyl phosphatidylcholine bilayer, Biochim. Biophys. Acta 550 (1979) 131–137.
[53] T. Wang, T. Mužić, A.D. Jackson, T. Heimburg, The free energy of biomembrane and nerve excitation and the role of anesthetics, Biochim. Biophys. Acta 1860 (2018), https://doi.org/10.1016/j.bbamem.2018.04.003.
[54] H. Zhang, Q. Fan, Y.E. Wang, C.R. Neal, Y.Y. Zuo, Comparative study of clinical pulmonary surfactants using atomic force microscopy, Biochim. Biophys. Acta 1808 (2011) 1832–1842.
[55] H.W. Taeusch, K. Lu, D. Ramierez-Schrempp, Improving pulmonary surfactants, Acta Pharm. Sin. 23 (2002) 11–15.
[56] S.B. Madsen, Thermodynamics of Nerves, Master's thesis University of Copenhagen, 2011.
[57] F. Tounsi, The Correlation Between Critical Anaesthetic Dose and Melting Temperatures in Synthetic Membranes. With Comments on the Possible Implications of the Soliton Model on Epilepsy, Master's thesis University of Copenhagen, 2015.
[58] T. Muzic, The Effect of Anesthetics on Phase Transitions in Biological Membranes, Master's thesis Niels Bohr Institute, University of Copenhagen, 2016.
[59] U.R. Pedersen, G.H. Peters, T.B. Schrøder, J.C. Dyre, Correlated volume-energy fluctuations of phospholipid membranes: a simulation study, J. Phys. Chem. B 114 (2010) 2124–2130.
[60] E.A. Evans, Bending resistance and chemically induced moments in membrane bilayers, Biophys. J. 14 (1974) 923–931.
[61] T. Heimburg, Phase transitions in biological membranes, in: C. Demetzos, N. Pippa (Eds.), Thermodynamics and Biophysics of Biomedical Nanosystems, Series in BioEngineering, Springer Nature, 2019, pp. 39–61.
[62] L. Onsager, Reciprocal relations in irreversible processes. II. Phys. Rev. 38 (1931) 2265–2279.
[63] H.M. Seeger, A. Alessandrini, P. Facci, KcsA redistribution upon lipid domain formation in supported lipid bilayers and its functional implications, Biophys. J. 98 (2010) 371a.
[64] C.A. Royer, Revisiting volume changes in pressure-induced protein unfolding, Biochim. Biophys. Acta 1595 (2002) 201–209.
[65] R. Ravindra, R. Winter, On the temperature - pressure free-energy landscape of proteins, Chem. Phys. Chem. 4 (2003) 359–365.
[66] J. Perez-Gil, T.E. Weaver, Pulmonary surfactant pathophysiology: current models and open questions, Physiology 25 (2010) 132–141.
[67] M. Echaide, C. Autilio, R. Arroyo, J. Perez-Gil, Restoring pulmonary surfactant membranes and films at the respiratory surface, Biochim. Biophys. Acta 1859

(2017) 1725–1739.
[68] B. Rudolph, K.M. Gebendorfer, J. Buchner, J. Winter, Evolution of *Escherichia coli* for growth at high temperatures, J. Biol. Chem. 285 (2010) 19029–19034.
[69] S. Guyot, L. Pottier, A. Hartmann, M. Ragon, J.H. Tiburski, P. Molin, E. Ferret, P. Gervais, Extremely rapid acclimation of *Escherichia coli* to high temperature over a few generations of a fed-batch culture during slow warming, MicrobiologyOpen 3 (2013) 52–63.
[70] H. Träuble, M. Teubner, P. Woolley, H. Eibl, Electrostatic interactions at charged lipid membranes. I. Effects of pH and univalent cations on membrane structure, Biophys. Chem. 4 (1976) 319–342.
[71] T. Heimburg, A.D. Jackson, Thermodynamics of the nervous impulse, in: K. Nag (Ed.), Structure and Dynamics of Membranous Interfaces, Wiley, 2008.
[72] K.L. Højholt, T. Mužić, S.D. Jensen, M. Bilgin, J. Nylandsted, T. Heimburg, S.K. Frandsen, J. Gehl, Calcium electroporation and electrochemotherapy for cancer treatment: importance of cell membrane composition investigated by lipidomics, calorimetry and in vitro efficacy, Sci. Rep. 9 (2019) 4758.
[73] R.J. Pedersen, Electrophysiological Measurements of Spontaneous Action Potentials in Crayfish Nerve in Relation to the Soliton Model, Master's thesis University of Copenhagen, 2011, http://membranes.nbi.dk/thesis-pdf/2011_Masters_RolfPedersen.pdf.
[74] L.D. Mosgaard, A.D. Jackson, T. Heimburg, Fluctuations of systems in finite heat reservoirs with applications to phase transitions in lipid membranes, J. Chem. Phys. 139 (2013) 125101.
[75] L.D. Mosgaard, K.A. Zecchi, T. Heimburg, Mechano-capacitive properties of polarized membranes, Soft Matter 11 (2015) 7899–7910.
[76] K.A. Zecchi, L.D. Mosgaard, T. Heimburg, Mechano-capacitive properties of polarized membranes and the application to conductance measurements of lipid membrane patches, J. Phys. Conf. Ser. 780 (2017) 012001.
[77] J.R. Hazel, Thermal adaptation in biological membranes: is homeoviscous adaptation the explanation? Ann. Rev. Physiol. 57 (1995) 19–42.
[78] J.R. Hazel, Influence of thermal acclimation on membrane lipid composition of rainbow trout liver, Am. J. Phys. Regul. Integr. Comp. Phys. 287 (1979) R633–R641.
[79] L.O. Ingram, Changes in lipid composition of *Escherichia coli* resulting from growth with organic solvents and with food additives, Appl. Environ. Microbiol. 33 (1977) 1233–1236.
[80] E.F. DeLong, A.A. Yayanos, Adaptation of the membrane lipids of a deep-sea bacterium to changes in hydrostatic pressure, Science 228 (1985) 1101–1103.
[81] T. Baumgart, S.T. Hess, W.W. Webb, Imaging coexisting fluid domains in biomembrane models coupling curvature and line tension, Nature 425 (2003) 821–824.
[82] A. Hac, H. Seeger, M. Fidorra, T. Heimburg, Diffusion in two-component lipid membranes–a fluorescence correlation spectroscopy and Monte Carlo simulation study, Biophys. J. 88 (2005) 317–333.
[83] M. Lösche, E. Sackmann, H. Möhwald, A fluorescence microscopic study concerning the phase diagram of phospholipids, Ber. Bunsenges. Phys. Chem. 87 (1983) 848–852.
[84] H.M. McConnell, V.T. Moy, Shapes of finite two-dimensional lipid domains, J. Phys. Chem. 92 (1988) 4520–4525.
[85] C.M. Knobler, Seeing phenomena in flatland: studies of monolayers by fluorescence microscopy, Science 249 (1990) 870–874.
[86] M. Gudmand, M. Fidorra, T. Bjørnholm, T. Heimburg, Diffusion and partitioning of fluorescent lipid probes in phospholipid monolayers, Biophys. J. 96 (2009) 4598–4609.
[87] P.F. Almeida, The many faces of lipid rafts, Biophys. J. 106 (2014) 1841–1843.
[88] D.A. Brown, E. London, Functions of lipid rafts in biological membranes, Ann. Rev. Cell Dev. Biol. 14 (1998) 111–136.
[89] M. Bagnat, S. Keranen, A. Shevchenko, K. Simons, Lipid rafts function in biosynthetic delivery of proteins to the cell surface in yeast, Proc. Natl. Acad. Sci. U. S. A. 97 (2000) 3254–3259.
[90] M. Bagnat, K. Simons, Lipid rafts in protein sorting and cell polarity in budding yeast *Saccharomyces cerevisiae*, Biol. Chem. 383 (2002) 1475–1480.
[91] M. Edidin, The state of lipid rafts: from model membranes to cells, Ann. Rev. Biophys. Biomol. Struct. 32 (2003) 257–283.
[92] S. Johnson, K.W. Miller, Antagonism of pressure and anaesthesia, Nature 228 (1970) 75–76.
[93] C.E. Overton, Studies of Narcosis, Chapman and Hall, New York, 1991 (English version of 'Studien der Narkose' from 1901).
[94] E. Gray, J. Karslake, B.B. Machta, S.L. Veatch, Liquid general anesthetics lower critical temperatures in plasma membrane vesicles, Biophys. J. 105 (2013) 2751–2759.
[95] I. Tasaki, K. Kusano, M. Byrne, Rapid mechanical and thermal changes in the garfish olfactory nerve associated with a propagated impulse, Biophys. J. 55 (1989) 1033–1040.
[96] K. Iwasa, I. Tasaki, Mechanical changes in squid giant-axons associated with production of action potentials, Biochem. Biophys. Res. Commun. 95 (1980) 1328–1331.
[97] K. Iwasa, I. Tasaki, R.C. Gibbons, Swelling of nerve fibres associated with action potentials, Science 210 (1980) 338–339.
[98] A. Gonzalez-Perez, L.D. Mosgaard, R. Budvytyte, E. Villagran Vargas, A.D. Jackson, T. Heimburg, Solitary electromechanical pulses in lobster neurons, Biophys. Chem. 216 (2016) 51–59.